PNAS
www.pnas.org

Supplementary Information for

Connectional architecture of a mouse hypothalamic circuit node controlling social behavior

Liching Lo[a,b,c,*], Shenqin Yao[d,*], Dong-Wook Kim[a,c], Ali Cetin[d], Julie Harris[d], Hongkui Zeng[d], David J. Anderson[a,b,c,1], and Brandon Weissbourd[a,b,c,1]

[a]Division of Biology and Biological Engineering, 156-29
California Institute of Technology, Pasadena, CA 91125, USA
[b]Howard Hughes Medical Institute
[c]Tianqiao and Chrissy Chen Institute for Neuroscience
[d]Allen Institute for Brain Science, Seattle, WA 98109, USA
[*]These authors contributed equally
[1]Correspondence: wuwei@caltech.edu, bweissb@gmail.com

This PDF file includes:

Supplemental Methods
Figs. S1 to S4
Tables S1 to S7
References for SI reference citations

www.pnas.org/cgi/doi/10.1073/pnas.1817503116

Supplemental Methods

Animals and Viral Vectors

Esr1$^{Cre/+}$ mice (see reference(1)) were generated and maintained at the California Institute of Technology (Caltech). vGAT-Cre and vGLUT2-Cre mice were obtained from Jackson Laboratory. All animal experiments were performed in accordance with NIH guidelines and approved by the Caltech Institutional Animal Care and Use Committee (IACUC). Viral vectors: (1) For the anterograde projection study, AAV1-CAG-FLEX-EGFP (titer ~8x10^{12} viral genomes(vg)/ml) were obtained from the University of Pennsylvania Gene Therapy Program. (2) For the retrograde input study, Cre-dependent AAV1-Syn-DIO-TVA66T-dTom-CVS-N2cG (titer ~4x10^{13} vg/ml), AAV1-Syn-DIO-TVA66T-dTom (titer ~4x10^{13} vg/ml), and pseudotyped, G-deleted rabies viruses (EnvA-CVS-N2c-histone-GFP, 5 x10^{9} infectious units (IU)/ml) were obtained from our collaborators at the Allen Institute for Brain Science (AIBS). (3) For the anterograde trans-neuronal tracing study, Cre-dependent HSV1-H129ΔTK-TT (see reference (2)) was kindly provided by Lynn Enquist (Princeton University) with titer ~7 x10^{9} plaque-forming units (pfu)/ml. (4) For the collateral projection study, Cre-dependent retrograde HSV-hEF1-α-LS1L-mCherry-IRES-flpo HT (titer ~3 x10^{9} IU/ml) was obtained from Massachusetts Institute of Technology (MIT) McGovern Institute for Brain Research. AAVDJ-EF1α-fDIO-EYFP was obtained from the University of North Carolina at Chapel Hill Gene Therapy Center Vector Core (titer ~4 x10^{12} vg/ml). (5) For tracing inputs based on projection (TRIO, see reference(3)), FLP-dependent AAVDJ-CAG-fDIO-TVA-mCherry (titer ~2 x 10^{13} vg/ml) and FLP-dependent AAV8-CAG-fDIO-RG (titer ~4 x10^{12} vg/ml) were obtained from the Stanford University Neuroscience Gene Vector and Virus Core. Pseudo-typed, G-deleted rabies EnvA-ΔG-B19-GFP (titer ~4x10^{8} transforming units (TU)/ml) were purchased from the Salk Institute Viral Vector Core. Pseudo-typed, G-deleted rabies EnvA-N2c-GFP (titer ~2 x 10^{8} IU/ml) were kindly provided by HHMI Janelia Virus Service Facility. Cre-dependent retrograde HSV-hEF1-α-LS1L-BFP-IRES-flpo HT for TRIO and Cre-dependent retrograde HSV-hEF1-α-LS1L-mCherry/GFP for duel retrograde labeling were obtained from MIT McGovern Institute for Brain Research.

Stereotaxic Surgery, Virus Injections, and immunohistochemistry

Esr1^{cre} mice (8-12 weeks old, male and female) were anaesthetized with 3-5% isoflurane for induction and 1-3% for maintenance. Mice were mounted on a stereotaxic frame (David Kopf Instruments) with heating pad placed underneath. For anterograde tracing, AAV1-FLEX-EGFP viruses were injected by iontophoresis (3 μA at 7 s 'on' and 7 s 'off' cycles for 5 min total) with a pulled glass capillary (World Precision Company) into VMHvl^{Esr1}. Region of interest (ROI) was positioned using Model 1900 Stereotaxic Alignment System (David Kopf Instruments). For VMHvl, coordinates are anteroposterior (AP): −1.5 mm from Bregma; mediolateral (ML): +0.78 mm from the midline, dorsoventral (DV): −5.775 mm. Mice were euthanized four weeks later with Ketamine (100 mg/kg) and Xylazine (10 mg/kg) and brains were analyzed by TissueCyte 1000 serial two-photon (STP) tomography system at AIBS.

For monosynaptic retrograde labeling, AAV1-DIO-TVA66T-dTom-N2cG (or AAV1-DIO-TVA66T-dTom for rabies glycoprotein-less control) viruses were injected by iontophoresis (3 μA at 7 s 'on' and 7 2 'off' cycles for 5 min total) into the VMHvl of Esr1-cre male mice, followed by ~500 nl of rabies EnvA-N2c-histone-GFP with a Nanoliter 2010 injector (World Precision Company) three weeks later into the same location. Mice were euthanized 9 days later

and brains were analyzed by TissueCyte 1000 serial two-Photon (STP) tomography system at AIBS.

For the glutamatergic and GABAergic inputs study, ~200 nl of HSV-LS1L-mCherry virus was injected into the VMHvl of vGLUT2-cre or vGAT-cre male mice (same coordinates as above, except ML= −0.78 for these and for injections described below). Mice were euthanized ~3 weeks later via perfusion with 4% PFA and serial sections were generated using a cryostat.

For poly-synaptic anterograde tracing, ~150-300 nl of HSV1-H129ΔTK-TT viruses were injected into the VMHvl of Esr1-cre male mice with a Nanoliter injector and mice were euthanized between 40 to 48 hours after injection depending on assessments of their health. Ketoprofen (5 mg/kg, SQ) was given each day until euthanization. To visualize tdTomato encoded by HSV1-H129ΔTK-TT tracers, sections were stained with rat anti-mCherry (Thermo Fisher Scientific, clone 16D7, Cat# M11238, RRID:AB_253661, 1:200) overnight at 4 C, followed by Alexa-488-donkey anti-rat (Invitrogen, 1:200) at room temperature for 3 hours. For the collateral projection study, ~200 nl of HSV-LS1L-flpo viruses were injected into projection targets of $VMHvl^{Esr1}$ neurons of Esr1-cre male mice (LSv coordinates, AP= +0.14, ML= −0.55, DV= −4; PAG coordinates, AP= −3.88, ML= −0.137, DV= −2.375; MPOA coordinates, AP= +0.02, ML= -0.3, DV= -5.375). At the same time, ~200 nl of FLP-dependent AAVDJ-fDIO-EYFP was injected into the VMHvl. Mice were perfused with 4% PFA 28-30 days after injection and serial sections were made using a cryostat.

For the projection-based input study, ~100-150 nl of HSV-LS1L-flpo viruses were injected into the projection targets (MPOA or PAG) of $VMHvl^{Esr1}$ neurons in Esr1-cre male mice. At the same time, a 1:1 mixture of AAVDJ-fDIO-TVA and AAV8-fDIO-RG viruses were injected into the VMHvl (~150 nl total). Three weeks later, rabies EnvA- ΔG-GFP was injected into the same location. Mice were euthanized 6 days later via perfusion with 4% PFA and serial sections were generated using a cryostat.

For duel-retrograde labeling, 200 nl of HSV-LS1L-mCherry and 200 nl of HSV-LS1L-EYFP was injected into the PAG and MPOA, respectively, in the same $VMHvl^{Esr1}$ male mouse. Mice were euthanized ~3 weeks later via perfusion with 4% PFA and serial sections were generated using a cryostat.

In all experiments, we targeted the Esr1+ cluster of the VMHvl, which forms a continuous population with the neighboring Tuberal nucleus (TU). The average % of viral back-labeled cells in these two regions combined was 77% from 8 injected mice selected from across experiments. The remaining labeling could be found in other nearby regions that express Esr1, particularly the ventral premammillary nucleus (PMv) and Arcuate Hypothalamic nucleus (ARC).

Image Acquisition and Analysis

For projection and input studies, through collaborations with AIBS, brain samples with GFP-labeled axonal projections or rabies-labeled cells were imaged using the TissueCyte 1000 serial two Photon (STP) tomography system (0.35 μm *x*-*y* resolution and 100 μm *z*-sampling interval) (see references (4, 5)). For quantification of projection strength or input neuron number, ROIs were selected and screenshots taken at the same magnification. Projection mapping images are publicly available and can be found at (http://connectivity .brain-map.org). Experiments used in the projection study are Experiments #176886958, #264248605, 264319363 posted on AIBS website (© 2015 Allen Institute for Brain Science. Allen Brain Atlas API. Available from: brain-map.org/api/index.html). Both Allen Mouse Brain Atlas (2004) and Allen Mouse Brain

Connectivity Atlas (2011) were used in this study. Thirty ROIs were chosen based on (1) projection or input strength, (2) relative position, located anteriorly or posteriorly, to VMHvl, (3) research interests in psychiatric disorders and innate behaviors. For anterograde trans-neuronal tracing, collateral projections, glutamatergic vs. GABAergic inputs (INSERT), and projection-based TRIO, images were acquired by confocal microscopy for starter cell images (Oympus FluoView FV1000), or by slide scanner for the quantification of starter cell location and labeling outside of the VMHvl (Olympus VS-ASW-S6). For quantification, matching images of ROIs were obtained using the "Crop to Clipboard" function of the slide scanner software. Twenty-eight ROIs (glutamatergic or GABAergic inputs), twenty ROIs (collateral projection), twelve ROIs (H129 transsynaptic anterograde tracing), and twenty-nine ROIs (TRIO) were chosen based on the criteria listed above. Additionally, for H129 labeling, SUBv, TTd, SFO, and SCH were chosen as we observed strong polysynaptic labeling.

For quantification of projections, images were analyzed using Fiji/ImageJ by manually setting a threshold (common to all images) to the point that tissue autofluorescence was not visible followed by identification of objects using particle analysis ("analyze particles" function), binarization of the image, and summation of the total positive area (i.e. the area that is covered by projections above threshold). For quantification of input/output cell number, images were processed as described for projection analysis, except watershed-based identification of objects was used prior to particle analysis which was used for object counting, with size and circularity limited to an appropriate range to identify individual cells. Automatic particle counting was visually inspected for accuracy and manually adjusted. For all ImageJ analysis, normalized projection strength or inputs were taken from three adjacent sections 30 or 60 μm apart. For cell size and fiber mass quantifications, confocal images (60x) obtained using an Olympus FluoView 1000 confocal were analyzed using Imaris Image Analysis Software (Bitplane, Oxford Instruments). To obtain optical image quality, stacked 60x confocal images of VMVHvl neurons were saved as OIB files and 3-D reconstructed using Imaris processing software followed by automated identification and quantification of fluorescent objects based on manually identified criteria (cells: volume threshold 100 μm^3; fibers: volume threshold 10 to 100 μm^3).

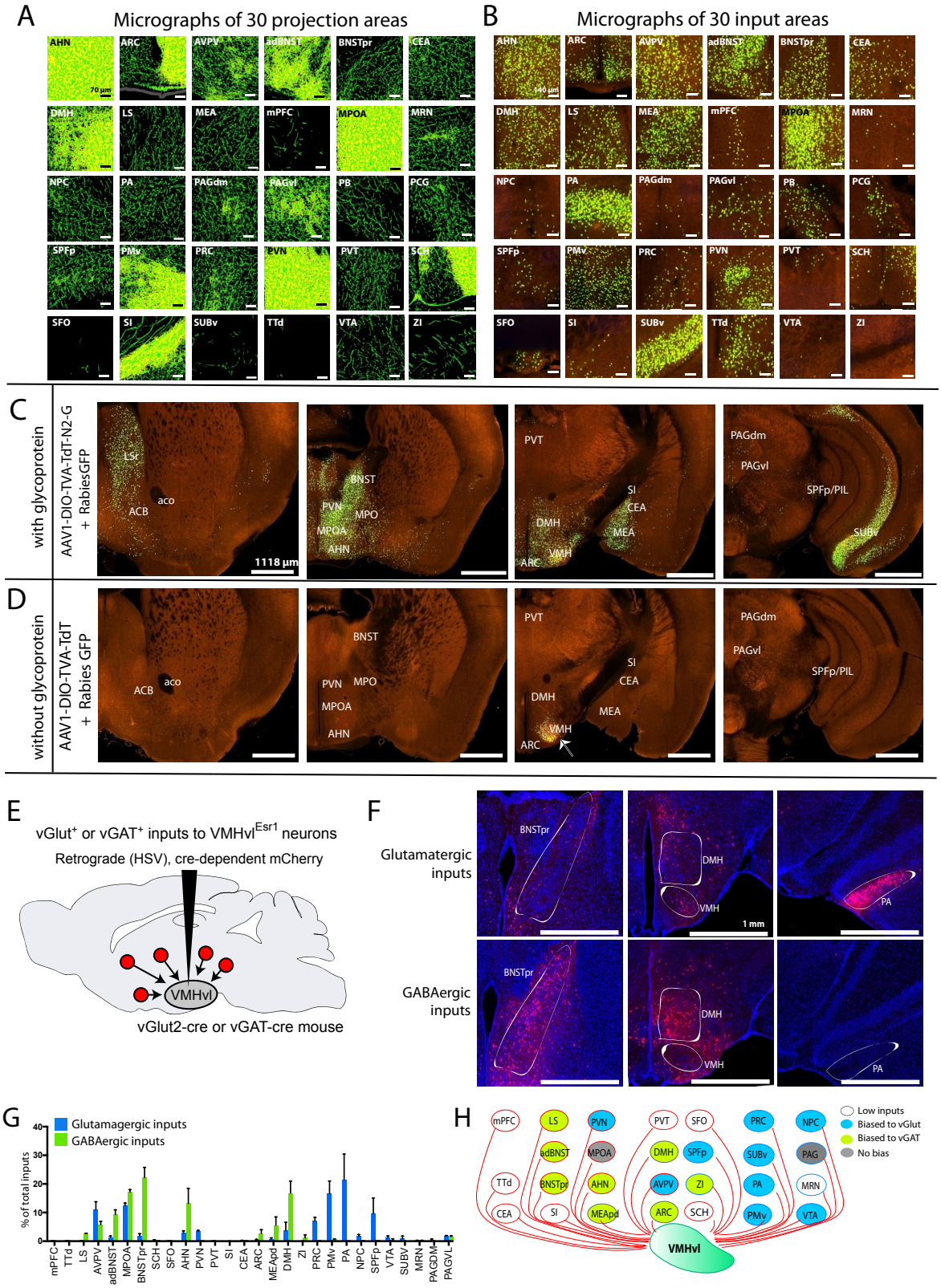
A
Micrographs of 30 projection areas
B
Micrographs of 30 input areas
AHN
ARC
AVPV
adBNST
BNSTpr
CEA
DMH
LS
MEA
mPFC
MPOA
MRN
NPC
PA
PAGdm
PAGvl
PB
PCG
SPFp
PMv
PRC
PVN
PVT
SCH
SFO
SI
SUBv
TTd
VTA
ZI
70 µm
140 µm
C
with glycoprotein
AAV1-DIO-TVA-TdT-N2-G
+ RabiesGFP
LSr
aco
ACB
1118 µm
BNST
PVN
MPO
MPOA
AHN
PVT
SI
CEA
DMH
MEA
VMH
ARC
PAGdm
PAGvl
SPFp/PIL
SUBv
D
without glycoprotein
AAV1-DIO-TVA-TdT
+ Rabies GFP
ACB
aco
BNST
PVN
MPO
MPOA
AHN
PVT
SI
CEA
DMH
MEA
VMH
ARC
PAGdm
PAGvl
SPFp/PIL
E
vGlut+ or vGAT+ inputs to VMHvlEsr1 neurons
Retrograde (HSV), cre-dependent mCherry
VMHvl
vGlut2-cre or vGAT-cre mouse
F
Glutamatergic inputs
GABAergic inputs
BNSTpr
DMH
VMH
1 mm
PA
G
Glutamagergic inputs
GABAergic inputs
% of total inputs
40
30
20
10
0
mPFC
TTd
LS
AVPV
adBNST
MPOA
BNSTpr
SCH
SFO
AHN
PVN
PVT
SI
CEA
ARC
MEApd
DMH
ZI
PRC
PMv
PA
NPC
SPFp
VTA
SUBV
MRN
PAGDM
PAGVL
H
mPFC
LS
PVN
PVT
SFO
PRC
NPC
adBNST
MPOA
DMH
SPFp
SUBv
PAG
TTd
BNSTpr
AHN
AVPV
ZI
PA
MRN
CEA
SI
MEApd
ARC
SCH
PMv
VTA
VMHvl
Low inputs
Biased to vGlut
Biased to vGAT
No bias

Figure S1, related to Figure 1. Inputs to and outputs from VMHvl^{Esr1} neurons
(A, B) Images taken with serial two-photon tomography of 30 regions showing projections from (A) and inputs to (B) VMHvl^{Esr1} neurons. Image credit (A): Allen Institute. Images are selected from Experiments #176886958, #264248605, 264319363 (see Methods). (C, D) Images from control experiments in which mice were injected with AAV-TVA66T with (C) or without (D) the rabies glycoprotein (RG). In mice without a supply of RG, there was no GFP labeling in any input regions except local GFP expression (arrow in D). (E) Schematic of experiment in which Cre-dependant, retrogradely-transported HSV-mCherry was injected into the VMH of either vGlut2-cre or vGAT-cre mice. (F) Representative images of glutamatergic (top panels) and GABAergic (bottom panels) inputs to VMHvl. (G) Proportion of total glutamatergic (blue bars) or GABAergic (green bars) input neurons in 28 areas analyzed (normalized to=100%, mean+SEM, n=2). (H) Schematic summarizing glutamatergic or GABAergic inputs to VMHvl.

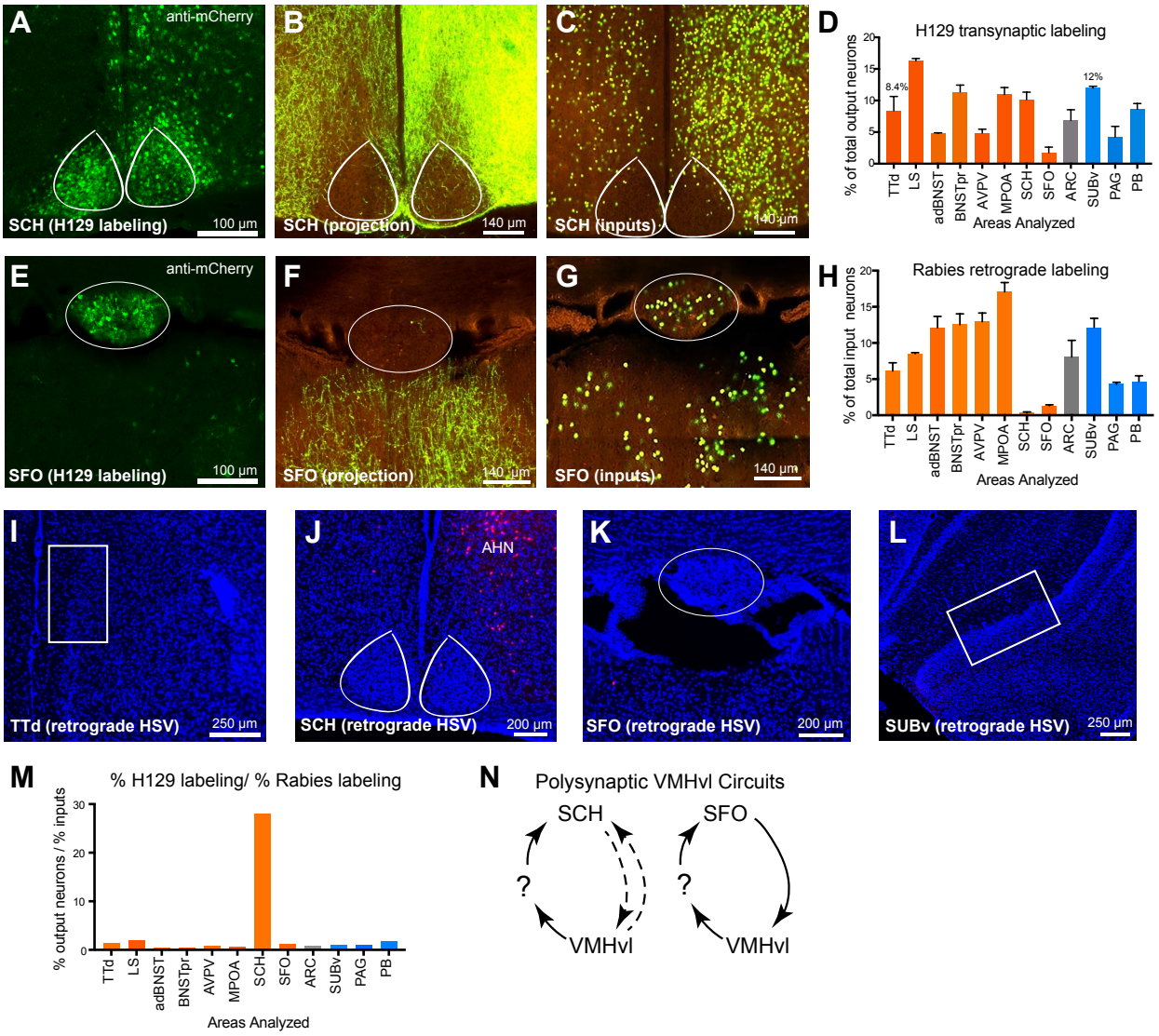

Figure S2, related to Figure 2. Indirect feedback loops revealed by anterograde trans-synaptic tracing

(A, E) Representative images of neurons labeled using the anterograde trans-synaptic tracer H129ΔTK-TT; (B, F) AAV-GFP labeled projections. (C, G) Rabies-GFP-labeled inputs. Note the minimal labeling of AAV-GFP projections (B, F) and input (C), but strong trans-synaptic labeling in (A, E). (D) Quantification showing the percent of H129ΔTK-TT labeled output neurons in each of 12 selected regions (n=2, same data as Fig. 2). (H) Quantification of proportion of inputs from 12 selected regions (mean+SEM, n=3). Data in (H) were extracted from Figure 1L and normalized to 100% using the same 12 regions for comparison to data in panel (D). (I-L) Control experiment for possible primary infection of axon terminals in anterograde tracing experiments in which a retrograde HSV (not HSV129) expressing cre-dependent mCherry was injected into the VMHvl of Esr1-cre mice. Little to no labeling is observed in the TTd, SCH, SFO, and SUBv. (M) Ratio of H129ΔTK-TT labeling to average input (i.e. data from D divided by data from H), for each region examined. Note the large ratio for SCH. (N) Schematic of indirect feedback loops from VMHvl^{Esr1} to SFO and indirect output to SCH.

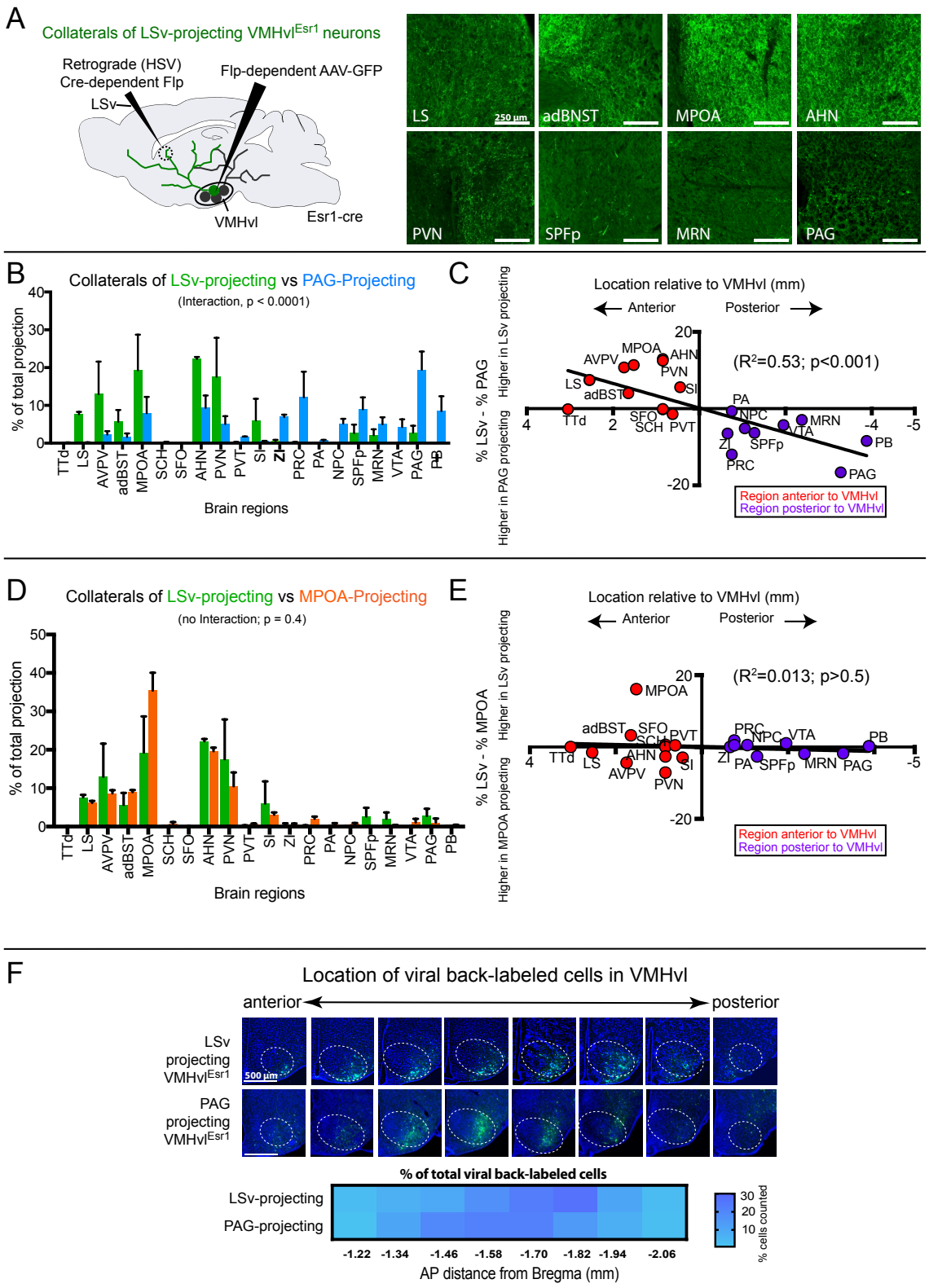
A
Collaterals of LSv-projecting VMHvl^{Esr1} neurons
Retrograde (HSV)
Cre-dependent Flp
Flp-dependent AAV-GFP
LSv
VMHvl
Esr1-cre
LS
250 µm
adBNST
MPOA
AHN
PVN
SPFp
MRN
PAG
B
Collaterals of LSv-projecting vs PAG-Projecting
(Interaction, p < 0.0001)
% of total projection
Brain regions
C
Location relative to VMHvl (mm)
Anterior
Posterior
(R²=0.53; p<0.001)
% LSv - % PAG
Higher in LSv projecting
Higher in PAG projecting
Region anterior to VMHvl
Region posterior to VMHvl
D
Collaterals of LSv-projecting vs MPOA-Projecting
(no Interaction; p = 0.4)
% of total projection
Brain regions
E
Location relative to VMHvl (mm)
Anterior
Posterior
(R²=0.013; p>0.5)
% LSv - % MPOA
Higher in LSv projecting
Higher in MPOA projecting
Region anterior to VMHvl
Region posterior to VMHvl
F
Location of viral back-labeled cells in VMHvl
anterior
posterior
LSv projecting VMHvl^{Esr1}
PAG projecting VMHvl^{Esr1}
500 µm
% of total viral back-labeled cells
LSv-projecting
PAG-projecting
-1.22 -1.34 -1.46 -1.58 -1.70 -1.82 -1.94 -2.06
AP distance from Bregma (mm)
% cells counted

Figure S3, related to Figure 3 and 4. VMHvl^{Esr1} subpopulations collateralize to multiple, distinct targets

(A) Schematic illustrating experimental strategy for labeling collaterals of VMHvl^{Esr1} neurons that project to the lateral septum (LSv). Representative images of coronal sections showing AAV-GFP expression in collateral projections of VMHvl^{Esr1} neurons that project to the LSv shown on the right. (B) Percent of total projection strength in each of 20 selected targets for VMHvl^{Esr1} neurons that project to the LSv (green bars, n=2) and VMHvl^{Esr1} neurons that project to the PAG (blue bars, n=3, data from Fig. 3). Bars show mean+SEM. There is a strong interaction effect by 2-way ANOVA ($p < 0.0001$). (C) Scatter plot of the location along the A-P axis relative to the VMHvl (x-axis) vs the difference in percent of total collaterals observed in each region between LSv- and PAG-projecting populations (percent of total for LSv minus percent of total for PAG; y axis). There is a significant correlation between AP position and bias towards LSv (anterior regions) vs PAG (posterior regions) ($R^2 = 0.53$, $p<0.001$). (D) Percent of total projection strength in each of 20 selected targets for VMHvl^{Esr1} neurons that project to the LSv (green bars, n=2, data same as in panel B) and VMHvl^{Esr1} neurons that project to the MPOA (orange bars, n=2, data from Fig. 3). Bars show mean+SEM. There is no interaction effect by 2-way ANOVA ($p = 0.4$). (E) Scatter plot of the location along the A-P axis relative to the VMHvl (x-axis) vs the difference in percent of total collaterals observed in each region between LSv- and MPOA-projecting populations (percent of total for MPOA – percent of total for PAG; y axis). There is no significant correlation between AP position and bias towards collaterals of LSv vs MPOA ($R^2 = 0.013$, $p>0.5$). (F) Images of viral labeling (top) and heatmap (bottom) showing the distribution of VMHvl neurons that project to the LSv and VMHvl neurons that project to the PAG along the A-P axis. LSv-projecting neuronal somata are distributed more posteriorly than PAG-projecting ones (n=2/e). Data for PAG and MPOA projecting populations in panels B-F are the same as in Fig. 3C and Fig. 4A.

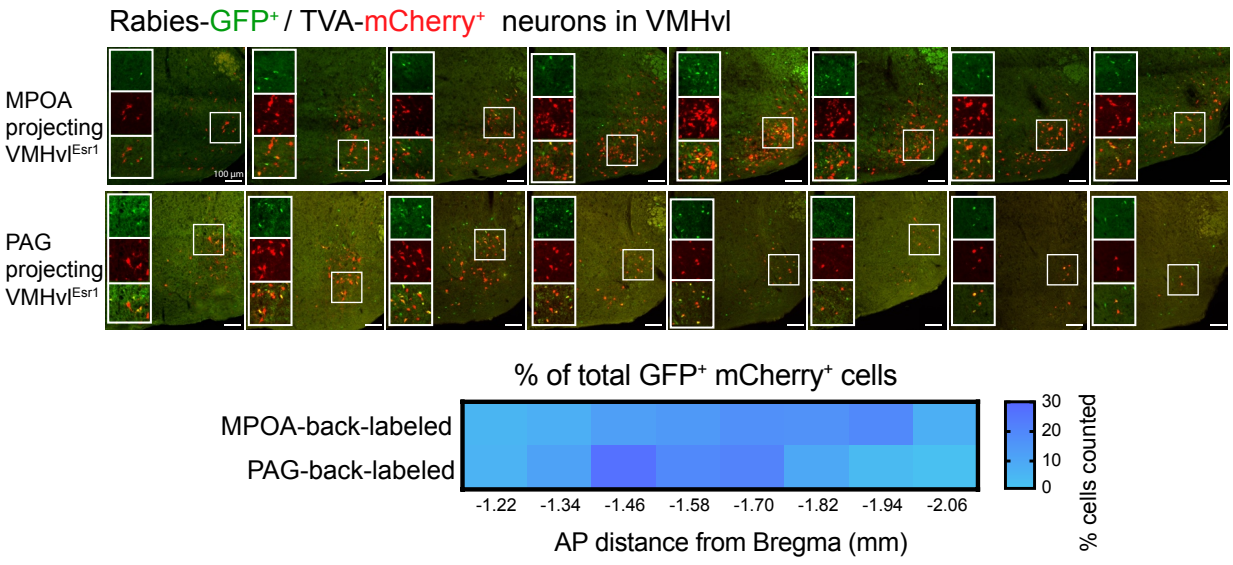

Figure S4, related to Figure 5. VMHvl^{Esr1} starter cell locations

Images (top) and heatmap (bottom) showing the distribution of VMHvl^{Esr1} starter cells from TRIO experiments - i.e. back-labeled either from the MPOA or PAG. Starter cell locations show a similar difference in A-P position as that seen in collateralization mapping experiments (cf. Fig. 4A). (n=2 for each population).

Abbreviation used	Full name
mPFC	Medial prefrontal cortex
PL	Prelimbic area
ILA	Infralimbic area
TTd	Taenia tecta, dorsal part
LS	Lateral septal nucleus
adBNST	Bed nuclei of the stria terminalis, anterior-dorsal division
BNSTpr	Bed nuclei of the stria terminalis, principal nucleus
MPOA	Medial preoptic area
SCH	Suprachiasmatic nucleus
SFO	Subfornical organ
AHN	Anterior Hypothalamic nucleus
PVN	Paraventricular hypothalamic nucleus
SI	Substantia innominata
CEA	Central amygdalar nucleus
ARC	Arcuate hypothalamic nucleus
MEA	Medial amygdalar nucleus
DMH	Dorsomedial nucleus of the hypothalamus
ZI	Zona incerta
PRC	Precommissural nucleus
PMv	Ventral premammillary nucleus
PA	Posterior amygdalar nucleus
NPC	Nucleus of the posterior commissure
SPFp	Subparafascicular nucleus, parvicellular part
PIL	Posterior intralaminar thalamic nucleus
VTA	Ventral tegmental area
SUBv	Subiculum, ventral part
MRN	Mid brain reticular nucleus
PAGdm	Periaqueductal gray, dorsomedial area
PAGvl	Periaqueductal gray, ventrolateral area
PB	Parabrachial nucleus
PCG	Pontine central gray

Table S1. Structures analyzed in this study and their abbreviations. Reference table showing abbreviations used in the text and figures of this study (left) and their full names (right).

Telencephalon		Esr1 projection	Canteras PHA-L
Orbitofrontal cortex	ORBm	+/-	-
Medial prefrontal cortex	mPFC	+/-	+/-
Dorsal peduncular cortex	DP	+/-	-
Tenia tecta, dorsal	TTd	+/-	-
Agranular insular cortex	AI	+/-	+/-
Perirhinal cortex	PERI	+/-	-
Ectorhinal cortex	ECT	+/-	-
Piriform cortex	PIR	+	+/-
Bed N. accessory olfactory N.	BA	+/-	-
N. diagonal band	NDB	++	+/-
Subfornical organ	SFO	+/-	-
Substantia Innominata	SI	+++	+
Medial septal N.	MS	++	-
Lateral septal N.	LS	++	++
Subiculum	SUB	+/-	-
Basolateral amygdala, anterior part	BLAa	++	++
Basolateral amygdala, posterior part	BLAp	++	++
Basal medial amygdala, anterior part	BMAa	++	++
Central amygdala	CEA	+++	++
Medial amygdala	MEA	+++	++
Posterior amygdala	PA	+	+/-
Amygdalo-piriform-transitional area	TR	+/-	-
Bed N. of stria terminalis, anterodorsal	adBST	+++	+++
Bed N. of stria terminalis, principal	BSTpr	+++	+++
Diencephalon			
Paraventricular N. of thalamus	PVT	++	+
Precomissural N.	PRC	++	-
Subparafascicular N. posterior part	SPFp	+	++
Parataenial N.	PT	++	-
Medial habenular N.	MH	+/-	-
Lateral habenular N.	LH	+	-
Mediodorsal thalamic N.	MD	++	+/-
Peripeduncular area	PP	+/-	+/-
Hypothalamus			
Median preoptic area	MEPO	++	+/-
Medial preoptic area	MPOA	+++	++++
Lateral preoptic area	LPO	+++	+
Supraoptic N.	SON	+/-	+/-
Suprachiasmatic N.	SCH	+	+
Retrochiasmatic N.	RCH	+++	++
Anterior hypothalamic N.	AHN	+++	++++
Paraventricular Hypothalamic N.	PVN	++	+++
Anteroventral periventricular N.	AVPV	+++	+
Periventricular N. of the hypothalamus	PV	+	+
Arcuate N.	ARC	++	+
Lateral hypothalamic N.	LHA	+++	+
Ventromedial hypothalamic N.	VMH	++	++++
Doromedial hypothalamic N.	DMH	++	+++
Ventral premammillary N.	PMv	+	+
Dorsal tuberomammillary N.	TMd	+/-	+/-
Supramamillary N.	SUM	++	+/-
Zona incerta	ZI	++	+
Posterior hypothalamic N.	PH	+++	++
Midbrain			
Periaqueductal gray, dorsomedial	PAGdm	++++	+++
Peraqueductal gray, ventrolateral	PAGvl	++++	+++
Midbrain reticular N.	MRN	+++	+
Cuneiform N.	CUN	+	+
Nucleus of the posterior commissure	NPC	+	+/-
Dorsal Raphe	DR	+	+/-
Ventral tegmental area	VTA	++	-
Hindbrain			
Locus Coeruleus	LC	+/-	+/-
Pontine central gray	PCG	+	-
Lateral parabrachial N.	LPB	++	+/-
Kolliker-Fuse subnucleus	KF	+/-	-

Table S2, related to Figure 1. Comparison between anterograde viral tracing of Esr1^{+} VMHvl neurons and previously published PHAL tracing from the VMHvl. Table comparing results in this paper to those of a previous study tracing VMHvl projections using PHAL (See reference(6)). Quantifications from this study were converted to discrete values for purposes of comparison (e.g. "++"). Regions with labeling in this study but not in Canteras et al. (1994) are highlighted in yellow.

Regions tested	Male #82	Male #209	Male Avg.±SEM	Female #95	Female #297	Female Avg.±SEM	TTEST btw males & females
PH	2.30%	2.65%	2.48%±0.18%	1.98%	1.51%	1.75%±0.24%	0.14
RE	1.24%	1.11%	1.18%±0.07%	1.12%	0.90%	1.01%±0.11%	0.35
DMH	3.92%	4.09%	4.01%±0.09%	3.79%	3.96%	3.88%±0.09%	0.39
PVT	0.96%	0.66%	0.81%±0.15%	0.95%	1.07%	1.01%±0.06%	0.39
PMd	0.48%	0.61%	0.55%±0.07%	0.09%	0.54%	0.32%±0.23%	0.49
CEA	2.01%	1.45%	1.73%±0.28%	1.81%	0.62%	1.22%±0.60%	0.54
RCH	2.20%	2.51%	2.36%±0.16%	2.15%	4.19%	3.17%±1.02%	0.57
PVpo	0.67%	0.86%	0.77%±0.10%	0.60%	2.20%	1.40%±0.80%	0.57
MS	1.24%	1.01%	1.13%±0.12%	1.12%	0.97%	1.05%±0.08%	0.63
VMH	2.30%	1.17%	1.74%±0.57%	1.55%	2.93%	2.24%±0.69%	0.63
LPO	4.11%	2.96%	3.54%±0.58%	4.91%	3.23%	4.07%±0.84%	0.66
MPO	7.46%	9.42%	8.44%±0.98%	7.84%	10.98%	9.41%±1.57%	0.66
MEA	2.87%	1.84%	2.36%±0.52%	2.58%	1.38%	1.98%±0.60%	0.68
LHA	14.26%	10.43%	12.35%±1.92%	13.09%	9.18%	11.14%±1.96%	0.70
LSr	2.58%	1.37%	1.98%±0.61%	3.27%	1.60%	2.44%±0.84%	0.70
PAG	10.43%	12.30%	11.37%±0.94%	13.35%	5.80%	9.58%±3.78%	0.72
SI	3.92%	2.54%	3.23%±0.69%	3.88%	1.46%	2.67%±1.21%	0.74
MRN	2.49%	2.03%	2.26%±0.23%	6.03%	0.73%	3.38%±2.65%	0.75
ZI	2.30%	1.56%	1.93%±0.37%	2.41%	0.82%	1.62%±0.80%	0.77
PVH	1.91%	2.47%	2.19%±0.28%	1.46%	3.49%	2.48%±1.02%	0.83
PVp	0.57%	0.91%	0.74±%0.17%	0.17%	1.75%	0.96%±0.79%	0.83
SCH	0.38%	0.62%	0.50%±0.12%	0.26%	0.92%	0.59%±0.33%	0.83
AVPV	0.48%	1.05%	0.77%±0.29%	0.43%	1.35%	0.89%±0.46%	0.84
PMv	0.38%	1.35%	0.87%±0.49%	0.34%	1.73%	1.04%±0.70%	0.86
BST	8.90%	11.49%	10.20%±1.30%	8.44%	11.21%	9.83%±1.39%	0.86
MPN	2.49%	4.49%	3.49%±1.00%	1.98%	5.73%	3.86%±1.88%	0.88
PVi	0.48%	0.55%	0.52%±0.04%	0.17%	0.79%	0.48%±0.31%	0.93
ARH	1.24%	1.52%	1.38%±0.14%	0.78%	1.88%	1.33%±0.55%	0.94
SCm	3.35%	2.33%	2.84%±0.51%	4.82%	1.09%	2.96%±1.87%	0.96
TU	2.97%	1.00%	1.99%±0.99%	1.55%	2.54%	2.05%±0.50%	0.96
AHN	7.27%	9.55%	8.41%±1.14%	5.68%	10.85%	8.27%±2.59%	0.97
SBPV	1.15%	1.21%	1.18±%0.03%	0.69%	1.72%	1.21%±0.52%	0.97
MEPO	0.67%	0.91%	0.79%±0.12%	0.69%	0.88%	0.79%±0.10%	0.98

Table S3, related to Figure 1. Projections of VMHvl Esr1^{+} neurons in males vs. females. Comparison between male and female mice of the proportion of total projection strength to each region analyzed. Values for individual mice (2/e male and female) shown followed by their average (see Methods). No significant differences were observed between male and female mice by pairwise t-tests for all regions analyzed.

Telencephalon		**Toth CTB**	**Rabies tracing**
Orbitofrontal cortex	ORBm	+/-	+/-
Medial prefrontal cortex	mPFC	++	++
Dorsal peduncular cortex	DP	+	+
Tenia tecta, dorsal	TTd	+	++
Agranular insular cortex	AI	+/-	+/-
Perirhinal cortex	PERI	+/-	+/-
Ectorhinal cortex	ECT	+/-	+/-
Piriform cortex	PIR	+/-	+/-
Bed N. accessory olfactory N.	BA	++	++
N. diagonal band	NDB	-	+/-
Subfornical organ	SFO	+/-	+/-
Substantia Innominata	SI	+/-	+/-
Medial septal N.	MS	-	-
Lateral septal N.	LS	++	+++
Subiculum	SUB	++++	++++
Basolateral amygdala, anterior part	BLAa	-	+/-
Basolateral amygdala, posterior part	BLAp	+	+
Basal medial amygdala, anterior part	BMAa	+/-	+/-
Central amygdala	CEA	-	+/-
Medial amygdala	MEA	++++	+++
Posterior amygdala	PA	++++	+++
Amygdalo-piriform-transitional area	TR	+	+
Bed N. of stria terminalis, anterodorsal	adBST	++++	++++
Bed N. of stria terminalis, principal	BSTpr	++++	++++
Diencephalon			
Paraventricular N. of thalamus	PVT	+	+
Precomissural N.	PRC	+/-	+
Subparafascicular N. posterior part	SPFp	+/-	+
Parataenial N.	PT	-	-
Medial habenular N.	MH	+/-	+/-
Lateral habenular N.	LH	-	-
Mediodorsal thalamic N.	MD	-	-
Peripeduncular area	PP	+/-	+/-
Hypothalamus			
Median preoptic area	MEPO	+	+
Medial preoptic area	MPOA	++++	++++
Lateral preoptic area	LPO	+++	+++
Supraoptic N.	SON	+	+
Striohypothalamic N.	StHY	+++	+++
Suprachiasmatic N.	SCH	+/-	+/-
Retrochiasmatic N.	RCH	+/-	+/-
Anterior hypothalamic N.	AHN	++	++++
Paraventricular Hypothalamic N.	PVN	++	+++
Anteroventral periventricular N.	AVPV	++	+++
Periventricular N. of the hypothalamus	PV	++	++
Arcuate N.	ARC	++	+++
Lateral hypothalamic N.	LHA	+/-	+
Ventromedial hypothalamic N.	VMH	+++	+++
Doromedial hypothalamic N.	DMH	++	+++
Ventral premammillary N.	PMv	++	++++
Dorsal tuberomammillary N.	TMd	++	++
Supramamillary N.	SUM	+/-	+/-
Zona incerta	ZI	-	+/-
Posterior hypothalamic N.	PH	++	++
Midbrain			
Periaqueductal gray, dorsomedial	PAGdm	+/-	+/-
Peraqueductal gray, ventrolateral	PAGvl	+/-	+/-
Midbrain reticular N.	MRN	-	+/-
Cuneiform N.	CUN	+/-	+/-
Nucleus of the posterior commissure	NPC	-	+/-
Dorsal Raphe	DR	+/-	+
Ventral tegmental area	VTA	+/-	+/-
Hindbrain			
Locus Coeruleus	LC	+/-	+/-
Pontine central gray	PCG	-	+/-
Lateral parabrachial N.	LPB	++	++
Kolliker-Fuse subnucleus	KF	+	+

Table S4, related to Figure 1. Inputs to VMHvl Esr1$^+$ neurons vs. previous CTB tracing of VMH inputs. Table comparing results in this paper using rabies virus to trace inputs to genetically-defined Esr1$^+$ neurons to those of a previous study tracing VMH inputs using CTB (see reference(7)). Quantifications from this study were converted to discrete values for purposes of comparison (e.g. "++"). Regions with labeling in this study but not in Toth et al. (2010) are highlighted in yellow.

Rank	Region	Inputs		Rank	Region	Projections	
		Average %	SEM (%)			Average %	SEM (%)
1	MPOA	8.89%	0.41%	1	AHN	9.51%	0.48%
2	AHN	7.91%	1.37%	2	MPOA	8.90%	0.97%
3	PMv	7.82%	1.04%	3	DMH	7.94%	0.42%
4	AVPV	6.77%	0.61%	4	PVN	7.63%	1.06%
5	BNSTpr	6.57%	0.75%	5	PMv	6.64%	0.35%
6	PA	6.46%	0.7%	6	PAGvl	5.92%	1.09%
7	SUBv	6.34%	0.64%	7	SI	5.60%	0.52%
8	adBNST	6.31%	0.67%	8	AVPV	5.41%	0.36%
9	MEA	5.44%	1.08%	9	adBNST	5.34%	1.38%
10	PVN	4.91%	0.32%	10	ARC	4.74%	0.84%
11	DMH	4.91%	0.58%	11	PAGdm	3.55%	0.20%
12	LS	4.44%	0.15%	12	PRC	3.06%	0.42%
13	ARC	4.18%	0.88%	13	BNSTpr	2.76%	0.67%
14	TTd	3.20%	0.51%	14	CEA	2.67%	0.12%
15	PB	2.43%	0.35%	15	PVT	2.48%	0.36%
16	SPFp	1.89%	0.53%	16	SPFp	2.46%	0.24%
17	PAGvl	1.81%	0.10%	17	NPC	2.13%	0.12%
18	CEA	1.62%	0.24%	18	PB	1.97%	0.24%
19	PCG	1.37%	0.22%	19	MRN	1.93%	0.12%
20	mPFC	1.30%	0.30%	20	PCG	1.86%	0.10%
21	PRC	1.21%	0.09%	21	LS	1.75%	0.18%
22	SI	0.85%	0.14%	22	PA	1.74%	0.19%
23	SFO	0.68%	0.07%	23	MEA	1.35%	0.08%
24	NPC	0.60%	0.19%	24	VTA	0.88%	0.30%
25	VTA	0.58%	0.21%	25	ZI	0.81%	0.21%
26	PAGdm	0.43%	0.08%	26	SCH	0.53%	0.06%
27	MRN	0.33%	0.05%	27	mPFC	0.27%	0.12%
28	ZI	0.28%	0.15%	28	SUBv	0.07%	0.04%
29	PVT	0.28%	0.06%	29	TTd	0.04%	0.02%
30	SCH	0.18%	0.04%	30	SFO	0.03%	0.01%

Table S5., related to Figure 1, inputs and outputs to VMHvl^{Esr1} neurons. Table showing percent of total input neurons and percent of total projection strength for the top 30 regions/each, rank-ordered by relative strength. Data were collected from micrographs of 3 adjacent sections per region per brain from three brains/each (see Methods). See Supplemental Figure 1 for micrographs.

Rank	Projection targets	Percent of total projections	Percent Of total Inputs	Ratio: projection/input
1	PVT	2.48%	0.28%	8.9
2	PAGdm	3.55%	0.43%	8.3
3	SI	5.60%	0.85%	6.6
4	MRN	1.93%	0.33%	5.8
5	NPC	2.13%	0.60%	3.6
6	PAGvl	5.92%	1.81%	3.3
Rank	Input regions	Percent of total Inputs	Percent of total projections	Ratio: inputs/projections
1	SUBv	6.34%	0.07%	90.6
2	TTd	3.20%	0.04%	80.0
3	SFO	0.68%	0.03%	22.7
4	mPFC	1.30%	0.27%	4.8
5	MEA	5.44%	1.35%	4.0
6	PA	6.46%	1.74%	3.7

Table S6., related to Figure 1, top six input-biased and output-biased regions. Table showing the regions that are most biased towards being projection targets of (left) versus sending inputs to (right) VMHvl Esr1^{+} neurons. See Table S5 for quantification of inputs and projections for each region.

Rank	Input pref.	Ratio input/ output	Dist. to Bregma (mm)	Top 10 output pref.	Ratio output/ input	Dist. to Bregma (mm)	No pref.	Dist. to Bregma (mm)	TTEST (col 4v7)	TTEST (col 4v9)	TTEST (col7v9)
1	SUBv	90.6	-3.78	PVT	8.9	-0.88	MPOA	0.02	**p=0.0297**	p=0.0997	p=0.7191
2	TTd	80	1.545	PAGdm	8.3	-4.78	ARC	-1.455			
3	SFO	22.7	-0.655	SI	6.6	-1.055	adBNST	0.145			
4	mPFC	4.8	1.945	MRN	5.8	-3.88	PB	-5.38			
5	MEA	4	-1.555	NPC	3.6	-2.555	AHN	-0.655			
6	PA	3.7	-2.255	PAGvl	3.3	-4.78	SPFp	-2.78			
7	LS	2.5	1.045	SCH	2.9	-0.655	PCG	-5.38			
8	BNSTpr	2.4	-0.18	ZI	2.9	-2.155	VTA	-3.455			
9	AVPV	1.3	0.245	PRC	2.5	-2.255	PVN	-0.655			
10	PMv	1.2	-2.255	CEA	1.6	-1.155	DMH	-1.555			

Table S7, related to Figure 1 and Table S5 and S6. Positional bias of input-preferred vs. output preferred regions. Table showing the top 10 input-biased (left) and output-biased (center) regions, and regions with no bias (right), their ratios of input to output strength, and their location relative to bregma. Pairwise t-tests show that there is a significant difference in the A-P location of input biased vs projection biased regions, with input-biased regions located anterior to projection-biased regions. No significant differences are observed when comparing biased regions to regions with no bias.

References

1. Lee H*, et al.* (2014) Scalable control of mounting and attack by Esr1+ neurons in the ventromedial hypothalamus. *Nature* 509(7502):627-632.
2. Lo L & Anderson DJ (2011) A Cre-dependent, anterograde transsynaptic viral tracer for mapping output pathways of genetically marked neurons. *Neuron* 72(6):938-950.
3. Schwarz LA*, et al.* (2015) Viral-genetic tracing of the input-output organization of a central noradrenaline circuit. *Nature* 524(7563):88-92.
4. Ragan T*, et al.* (2012) Serial two-photon tomography for automated ex vivo mouse brain imaging. *Nat Methods* 9(3):255-258.
5. Oh SW*, et al.* (2014) A mesoscale connectome of the mouse brain. *Nature* 508(7495):207-214.
6. Canteras NS, Simerly RB, & Swanson LW (1994) Organization of Projections From the Ventromedial Nucleus of the Hypothalamus: A *Phaseolus vulgaris*-Leucoagglutinin Study in the Rat. *The Journal of Comparative Neurology* 348:41-79.
7. Toth M, Fuzesi T, Halasz J, Tulogdi A, & Haller J (2010) Neural inputs of the hypothalamic "aggression area" in the rat. *Behav Brain Res* 215(1):7-20.